New Highly Divided Ce−Ca-Based Oxyfluorides with UV-Shielding Properties: Study of the $Ce_{1-x}Ca_xO_{2-x}$ and $Ce_{1-x}Ca_xO_{2-x-y/2}F_y$ Series

L. Sronek,[†] J. Majimel,[†] Y. Kihn,[‡] Y. Montardi,[§] A. Tressaud,[†] M. Feist,[||] C. Legein,[⊥] J.-Y. Buzaré,[#] M. Body,[#] and A. Demourgues*,[†]

ICMCB, CNRS, Université Bordeaux 1, 87 avenue du Dr. A. Schweitzer, 33608 Pessac Cedex, France, CEMES-CNRS, 29 rue Jeanne Marvig, BP 94347, 31055 Toulouse Cedex, France, Rhodia, Centre de Recherche d'Aubervilliers, 52 rue de la Haie-Coq, 93308 Aubervilliers Cedex, France, Institut für Chemie, Humboldt-Universität zu Berlin, Brook-Taylor-Strasse 2, D-12489 Berlin, Germany, Laboratoire des Oxydes et Fluorures, CNRS UMR 6010, Institut de Recherche en Ingénierie Moléculaire et Matériaux Fonctionnels, CNRS FR 2575, Université du Maine, avenue Olivier Messiaen, 72085 Le Mans Cedex 9, France, and Laboratoire de Physique de l'Etat Condensé, CNRS UMR 6087, Institut de Recherche en Ingénierie Moléculaire et Matériaux Fonctionnels, CNRS FR 2575, Université du Maine, avenue Olivier Messiaen, 72085 Le Mans Cedex 9, France

Received June 1, 2007. Revised Manuscript Received July 25, 2007

Coprecipitations of Ce(III) nitrates and Ca chlorides have been performed in basic medium at pH > 12 using NaOH, H_2O_2, and HF as fluorinating agent. Powders have been annealed under air at 600 °C during 12 h. Oxides and oxyfluorides with $Ce_{1-x}Ca_xO_{2-x}$ and $Ce_{1-x}Ca_xO_{2-x-y/2}F_y$ formulas have been obtained. The Ce/Ca and F/Ca atomic ratios have been determined by elemental analysis (microprobe analysis and F titration with specific electrode), leading one to conclude that the higher is the Ca content, the higher is the F rate. The F/Ca atomic ratio is always lower than 1, but the F content strongly increases with the Ca rate, demonstrating the affinity of fluorine for Ca atoms. XRD data analysis confirmed that Ce−Ca-based oxides and oxyfluorides crystallize with the fluorite-type structure (SG: $Fm\bar{3}m$) and the *a*-cell parameter follows Vegard's law both for oxide and for oxyfluoride series. The solubility limit has been estimated to correspond to a Ca/Ce atomic ratio between 0.35 and 0.40 thanks to an accurate XRD analysis using monochromatic Cu K_{α_1} radiation, which allows one to detect the occurrence of CaF_2 traces. Taking into account the F−Ce bond distance in tetrahedral coordination (bond valence model Ce−F = 2.50 Å; average bond distances in $Ce_{1-x}Ca_xO_{2-x-y/2}F_y$: Ce/Ca−O/F = 2.35 Å), the low value of the F/Ca atomic ratio is governed by steric effects and constrains present in the network. Finally, an accurate EELS analysis on isolated particles (10−20 nm) with $Ce_{0.75}Ca_{0.25}O_{1.67}F_{0.17}$ composition confirms the value of the Ca/Ce average atomic ratio, and preliminary ^{19}F MAS NMR investigations show the occurrence of various $FCa_{4-n}Ce_n$ environments ($0 \leq n \leq 0.4$). TEM analysis reveals that particle size is around 10 nm, which corresponds to the coherent domain/crystallite size determined by XRD analysis taking into account a Thompson−Cox−Hasting function for the X-ray diffraction lines shape. Finally, the $Ce_{1-x}Ca_xO_{2-x}$ and $Ce_{1-x}Ca_xO_{2-x-y/2}F_y$ series exhibit interesting UV-shielding properties with a decrease of the optical band gap with Ca content in the oxide series, whereas the band gap varies inversely with Ca and F content in the oxyfluoride series. This tendency has been interpreted considering the difference in the Ce^{4+} electropositive character in these two systems.

Introduction

Titanium dioxide (TiO_2), zinc oxide (ZnO), and cerium dioxide (CeO_2) exhibit optical band gap associated with the charge-transfer band at 3.1−3.25, 3.4, and 3.2 eV, respectively,[1−6] at the frontier between UV and visible range. Because of their high refractive index in the visible range, that is, around 2.75−2.45 for TiO_2[7] and CeO_2[8] compounds, synthesis of nanosized particles is necessary to ensure UV-shielding properties with a sufficient transparency. In addition, most of these oxides exhibit high photocatalytic or oxidation

* Corresponding author. E-mail: demourg@icmcb-bordeaux.cnrs.fr.
[†] Université Bordeaux 1.
[‡] CEMES-CNRS.
[§] Rhodia.
[||] Humboldt-Universität zu Berlin.
[⊥] Laboratoire des Oxydes et Fluorures, Université du Maine.
[#] Laboratoire de Physique de l'Etat Condensé, Université du Maine.

(1) Asahi, R.; Taga, Y.; Mannstadt, W.; Freeman, A. J. *Phys. Rev. B* **2000**, *61*, 7459−7465.
(2) Sorantin, P. I.; Schwarz, K. *Inorg. Chem.* **1992**, *31*, 567−576.
(3) Lindan, P. J. D.; Harrison, N. M.; Gillan, M. J.; White, J. A. *Phys. Rev. B* **1997**, *55*, 15919−15927.
(4) Goniakowski, J.; Holender, J. M.; Kantorovich, L. N.; Gillan, M. J.; White, J. A. *Phys. Rev. B* **1996**, *53*, 957−960.
(5) Karpina, V. A.; Lazorenko, V. I.; Lashkarev, C. V.; Dobrowolski, V. D.; Kopylova, L. I.; Baturin, V. A.; Pustovoytov, S. A.; Karpenko, A. J.; Eremin, S. A.; Lytvyn, P. M.; Ovsyannikov, V. P.; Mazurenko, E. A. *Cryst. Res. Technol.* **2004**, *39*, 980−992.
(6) Skorodumova, N. V.; Ahuja, R.; Simak, S. I.; Abrikosov, I. A.; Johansson, B.; Lundqvist, B. I. *Phys. Rev. B* **2001**, *64*, 115108.
(7) Rocquefelte, X.; Goubin, F.; Montardi, Y.; Viadère, N.; Demourgues, A.; Tressaud, A.; Whangbo, M.-H.; Jobic, S. *Inorg. Chem.* **2005**, *44*, 3589−3593.
(8) Goubin, F.; Rocquefelte, X.; Whangbo, M.-H.; Montardi, Y.; Brec, R.; Jobic, S. *Chem. Mater.* **2004**, *16*, 662−669.

10.1021/cm071482h CCC: $37.00
Published on Web 09/19/2007

catalytic activity, leading to the generation of reactive oxygen species and the degradation of various organics.[9−11] The substitution of various cations for Ce^{4+} or Ti^{4+} has been widely investigated either to enhance or to reduce the photocatalytic or oxidation catalytic activity.[12−15] Ca^{2+} substitution for Ce^{4+} ions in CeO_2 led to nanosized particles with a clear reduction of the oxidation catalytic activity of ceria.[16]

The Ce/Ca coprecipitation process was carried out from chloride precursors at neutral or basic pH, followed by oxidation with H_2O_2.[12] $Ce_{1-x}Ca_xO_{2-x}$ compositions with particle sizes around 5−10 nm exhibit UV-shielding properties with a slight reduction of the optical band gap as compared to the undoped oxide.[16] Yamashita et al.[12] suggested that the maximum solubility limit of CaO into CeO_2 is equal to or less than 30 mol %, corresponding to the formula $Ce_{0.7}Ca_{0.3}O_{1.7}$. Particle sizes decrease with Ca content, whereas strain parameters increase in good agreement with the occurrence of oxygen vacancies.[17] From $T = 600$ °C, the strain parameters decrease up to the formation of CaO at $T = 800$ °C, and the particle size strongly increases in this temperature range.[17] Moreover, electronic properties of $Ce_{1-x}Ca_xO_{2-x}$ oxides based on O K and Ce L_{III}-edges of XANES spectra and calculated density of states[17] reveal the reduction of 2p (O) − 4f (Ce) electronic transition energy with Ca doping with a cation charge redistribution where the Ca atoms become more electropositive than in CaO, while the Ce atoms are less electropositive than those in CeO_2. To reduce the refractive index in visible range and the electronic polarizability as well as the oxidation catalytic activity associated with the generation of oxygen species, F^- ions have been substituted for O^{2-} anions as Ca^{2+} ions for Ce^{4+} cations. Moreover, CeO_2 and CaF_2 compounds adopt the same fluorite-type structure with almost identical cell parameters equal to 5.41 (CeO_2)[18] and 5.46 Å (CaF_2),[19] respectively. Coprecipitations in highly basic and fluorinated medium have been attempted (pH > 12). XRD, chemical analysis, ^{19}F NMR, and TEM/EELS measurements have been carried out for an accurate characterization of $Ce_{1-x}Ca_xO_{2-x}$ and $Ce_{1-x}Ca_xO_{2-x-y/2}F_y$ compounds. Finally, the UV-shielding properties in both systems will be discussed. However, no photocatalytic and oxidation catalytic activity measurements have been performed on these series.

(9) Hoffmann, M. R.; Martin, S. T.; Choi, W.; Bahnemann, D. W. *Chem. Rev.* **1995**, *95*, 69−96.
(10) Fu, D. G.; Zhang, Y.; Wang, X.; Liu, J. Z.; Lu, Z. H. *Chem. Lett.* **2001**, 328−329.
(11) Trovarelli, A.; de Leitenburg, C.; Boaro, M.; Dolcetti, G. *Catal. Today* **1999**, *50*, 353−367.
(12) Yamashita, M.; Kameyama, K.; Yabe, S.; Yoshida, S.; Fujishiro, Y.; Kawai, T.; Sato, T. *J. Mater. Sci.* **2002**, *37*, 683−687.
(13) Yabe, S.; Sato, T. *J. Solid State Chem.* **2003**, *171*, 7−11.
(14) Dagan, G.; Sampath, S.; Lev, O. *Chem. Mater.* **1995**, *7*, 446−453.
(15) Takata, T.; Furumi, Y.; Shinohara, K.; Tanaka, A.; Hara, M.; Kondo, J. N.; Domen, K. *Chem. Mater.* **1997**, *9*, 1063−1064.
(16) Li, R.; Yabe, S.; Yamashita, M.; Momose, S.; Yoshida, S.; Yin, S.; Sato, T. *Solid State Ionics* **2002**, *151*, 235−241.
(17) Rodriguez, J. A.; Wang, X.; Hanson, J. C.; Liu, G.; Iglesias-Juez, A.; Fernandez-Garcia, M. *J. Chem. Phys.* **2003**, *119*, 5659−5669.
(18) Kümmerle, E. A.; Heger, G. *J. Solid State Chem.* **1999**, *147*, 485−500.
(19) Cheetham, A. K.; Fender, B. E. F.; Cooper, M. J. *J. Phys. C: Solid State Phys.* **1971**, *4*, 3107−3121.

Experimental Methods

1. Preparation of Ce−Ca-Based Oxides and Oxyfluorides. The Ce−Ca-based oxides and oxyfluorides were prepared by coprecipitation performed in basic medium at pH > 12. The starting materials are Ce(III) nitrates and Ca chlorides. Yamashita et al.[12] have already explored this route but only in the case of Ce−Ca-based oxides. In our case, the pH, which is a key parameter, was adjusted taking into account the respective domain of precipitation of hydroxides, and this route was also applied to oxyfluorides with a fitted stirring duration.

The Ce−Ca-based oxides synthesis consists of a simultaneous addition in deionized water at around 45 °C of $Ce(NO_3)_3 + CaCl_2$ aqueous solutions and a 4 M sodium hydroxide solution. After adjusting the pH at values higher than 12, the Ce^{3+} ions were oxidized into Ce^{4+} ions using hydrogen peroxide (30%). Next, the mixture was stirred during 3 or 20 h. In the case of the preparation of oxyfluorides, after the stirring step, the solution containing Ce−Ca hydroxides was added to a basic fluorinated solution (pH >12) prepared from HF (40%) and NaOH solutions with a precursor ratio equal to F/Ca = 2. This mixture was stirred during 1 h, the pH being under control all along the maturation of particles. The precipitate was collected after centrifugation and several washings with deionized water (pH = 6−7). Next, the as-recovered precipitates were dried at 100 °C during one night and finally annealed under air at 600 °C during 12 h. Crystalline compounds with pale yellow coloration were obtained.

2. Elemental Analysis. The Ce/Ca atomic ratio in the Ce−Ca-based oxides and oxyfluorides was determined by wavelength dispersive spectrometry (WDS) using a CECAMA SX 630 microprobe. The samples were pressed into disks to get a planar surface and so improve the response of the signal. The fluorine content was quantified by F^- titration with specific electrode at Analysis Central Service (SCA-CNRS, Vernaison, France). To determine the carbon content in the compounds, C−H−N−S microanalysis was performed on a Thermoelectron flash EA 1112 apparatus.

3. Magnetic Measurements. The magnetic susceptibilities χ were determined on a Superconducting Quantum Interference Device (SQUID) magnetometer. The magnetization M ($M = \chi^*H$) was determined on ∼130−150 mg of powdered sample in the temperature range 4−300 K with an applied field (H) of 4 T.

4. Thermal Behavior. Thermogravimetry analyses (TGA) were performed to identify the outgassed species and to study the thermal stability of oxides and particularly the oxyfluorides. Two kinds of experiments were undertaken. To reveal the nature of various species formed during the thermal analysis, a thermogravimetry analysis coupled with mass spectrometry (TGA-SM) was performed on an oxyfluoride. The measurements were carried out using a Netzsch thermoanalyzer STA 409C skimmer on 34−40 mg of the sample with a constant purge gas flow of 70 mL/min nitrogen and a constant heating rate of 10 °C/min up to 850 °C. Second, to compare the total weight loss, only TGA experiments were conducted on other oxyfluorides using a SETARAM MTB 10-8 apparatus with a constant purge gas flow of nitrogen and a heating rate of 3 °C/min up to 800 °C.

5. X-ray Diffraction. The compounds were characterized by X-ray powder diffraction using a Philips PW 1050 diffractometer in a Bragg−Brentano geometry with Cu K_α radiation (K_{α_1} = 1.54059 Å and K_{α_2} = 1.54441 Å). The intensity data were collected at room temperature over a 2θ range of 5−110° with 0.02° steps and integration time of 10 s. For some samples, a more accurate study was performed using monochromated Cu K_α radiation (K_{α_1} = 1.54059 Å). In this case, diffractograms were recorded on a PANalytical X'Pert Pro with Ge(111) incident beam monochromator. Data were collected over a range of 15−120° with 0.017°

Table 1. Elemental Analysis of Ce−Ca-Based Oxides (Microprobe Analysis)

sample	Ca/Ce precursor atomic ratio	Ca/Ce final atomic ratio	Na/Ce final atomic ratio
O1	0	0	0.094(1)
O2	0.04	0.053(1)	0.033(5)
O3	0.11	0.081(5)	0.018(4)
O4	0.20	0.207(4)	0
O5	0.28	0.273(4)	0
O6	0.39	0.33(1)	0
O7	0.54	0.414(4)	0

Table 2. Elemental Analysis of Ce−Ca-Based Oxyfluorides (Microprobe Analysis for Cations and Titration of F^- Ions by Specific Electrode)

sample	Ca/Ce precursor atomic ratio	Ca/Ce final atomic ratio	Na/Ce final atomic ratio	F/Ce final atomic ratio
F1	0.04	0.051(2)	0.035(6)	<0.01
F2	0.11	0.094(3)	0.013(2)	0.02(1)
F3	0.18	0.156(6)	0	0.03(1)
F4	0.28	0.252(5)	0	0.09(1)
F5	0.39	0.342(8)	0	0.23(1)
F6	0.54	0.410(4)	0	0.34(1)
F7[a]	0.54	0.40(3)	0	0.52(1)

[a] Mixture containing $Ce_{1-x}Ca_xO_{2-x-y/2}F_y$ and CaF_2.

steps. The lattice parameters and the crystallite sizes were determined by profile matching (Le Bail[20] fit) using the Thompson−Cox−Hastings[21] function with the Fullprof[22] program package.

6. ^{19}F NMR. The ^{19}F MAS NMR spectra were recorded on an Avance 300 Bruker spectrometer (7 T) with a Larmor frequency of 282.2 MHz for ^{19}F, using a high-speed CP MAS probe with a 2.5 mm rotor. The external reference chosen for isotropic chemical shift determination was C_6F_6 ($\delta_{iso}C_6F_6$ vs $CFCl_3 = -164.2$ ppm). Spectra were acquired using a single pulse sequence (1 μs), followed by the free induction decay acquisition. The delay between two acquisitions was 1 s. For such a delay, the quantitativity of the spectra was checked. The discrimination of isotropic peaks from spinning sidebands was achieved by recording spectra at spinning frequencies equal to 20 and 25 kHz. The spectra were reconstructed using the Dmfit software.[23]

7. Transmission Electron Microscopy (TEM). To examine the size and the morphology of particles, transmission electron microscopy (TEM) pictures were recorded using a microscope TECNAI F20 equipped with a field emission gun, operating at 200 kV with a point resolution of 0.24 nm. The powder in toluene suspension was placed on a copper mesh grid and dried in air. The pictures were realized in bright field.

8. Electron Energy Loss Spectroscopy. Moreover, to explore accurately the composition homogeneity of each grain, electron energy loss spectroscopy (EELS) spectra were recorded with a Philips CM20 microscope operating at 200 kV with a point resolution of 0.27 nm. The analyses were performed from the calcium $L_{2,3}$-edge, fluorine and oxygen K-edges, and cerium $M_{4,5}$-edge after subtracting the background. The samples were crushed in an agate mortar and dispersed on a copper grid covered by a holey carbon film.

9. Diffuse Reflectance Spectroscopy. Diffuse reflectance measurements were carried out in the UV−visible range from 200 to 800 cm^{-1} on a Cary spectrophotometer at room temperature to illustrate the UV-shielding properties of such compounds.

Table 3. Room-Temperature Magnetic Susceptibility of $Ce_{0.91}Na_{0.09}O_{1.87}$, $Ce_{0.75}Ca_{0.25}O_{1.75}$, and $Ce_{0.75}Ca_{0.25}O_{1.67}F_{0.17}$ Compositions and $Ce_2Sn_2O_7$, CeF_3, and CeO_2 as References

compositions	χ_m (emu/mol)
O1: $Ce_{0.91}Na_{0.09}O_{1.87}$	1.1×10^{-4}
O6: $Ce_{0.75}Ca_{0.25}O_{1.75}$	1.3×10^{-4}
F5: $Ce_{0.75}Ca_{0.25}O_{1.67}F_{1.17}$	1.2×10^{-4}
$Ce_2Sn_2O_7$[24]	3.1×10^{-3}
CeF_3	2.1×10^{-3}
CeO_2[25]	0.6×10^{-4}
CeO_2 (Alfa Products)	0.5×10^{-4}

Results and Discussion

1. Elemental Analysis. The compositions of Ce−Ca-based oxides (Oi samples) and oxyfluorides (Fi samples) are reported in Tables 1 and 2, respectively, where the Ca/Ce, Na/Ce, and F/Ce atomic ratios are given. The Ca/Ce precursor atomic ratios are also listed. In oxides as well as in oxyfluorides, the Ca/Ce atomic ratios determined on the final powder are generally lower than those of the Ca/Ce precursor. This feature illustrates the importance of the pH during the synthesis. Indeed, to improve the Ca^{2+} substitution for Ce^{4+} ions, the pH must be as high as possible because of the solubility constant of respective hydroxides. The precipitation of $Ca(OH)_2$ begins indeed at pH higher than 11.5. Moreover, it is not excluded that washing with deionized water at pH = 6−7 leads to the elimination of Ca^{2+} ions due to the high solubility of Ca^{2+} ions under pH = 7.

The F/Ca atomic ratio in Table 2 increases with the Ca/Ce atomic ratio in good agreement with the affinity of fluorine for calcium atoms. Yet whereas the F/Ca precursor atomic ratio is equal to 2, the F/Ca atomic ratio in the final product is always lower than 1. However, it is not the case of sample F7, which was defined on the basis of an accurate XRD analysis as a mixture of Ce−Ca-based oxyfluoride and CaF_2, discussed in a following section.

Otherwise, coming from NaOH addition, Na^+ ions have been detected in samples with the lowest Ca contents, so that the (Ca + Na)/Ce atomic ratio is always lower than 0.10. It can be thus considered in a first step that alkaline and alkaline-earth cations are substituted for Ce^{4+} cations. In a recent ^{23}Na NMR study, which will be published later, on such Ce-based compounds adopting fluorite-type structure, the recorded spectra present characteristic features of electric field gradient and isotropic chemical shift distributions (asymmetry of the central line and broadening of the spinning side bands). This is in agreement with the occurrence of Na^+ disordered environments with various numbers of O^{2-} and F^- anions at different distances surrounding Na^+ cations.

In the oxyfluoride series, two samples F6 and F7 have the same Ca/Ce atomic ratio (0.40), but the F/Ce atomic ratio is higher for F7 (0.52), leading to a mixture of Ca−Ce oxyfluorides and CaF_2 as previously mentioned. In the case of F6, the F/Ce atomic ratio is equal to 0.34, and CaF_2 was not detected as in the other oxyfluorides with lower Ca contents. This difference illustrates the importance of the

(20) Le Bail, A.; Louër, D. *J. Appl. Crystallogr.* **1978**, *11*, 50−55.
(21) Thompson, P.; Cox, D. E.; Hastings, J. B. *J. Appl. Crystallogr.* **1987**, *20*, 79−83.
(22) Carjaval, J. R. FULLPROF Program, Rietveld Pattern Matching Analysis of Powder Patterns, ILL, Grenoble, 1990.
(23) Massiot, D.; Fayon, F.; Capron, M.; King, I.; Le Calvé, S.; Alonso, B.; Durand, J. O.; Bujoli, B.; Gan, Z.; Hoatson, G. *Magn. Reson. Chem.* **2002**, *40*, 70−76.

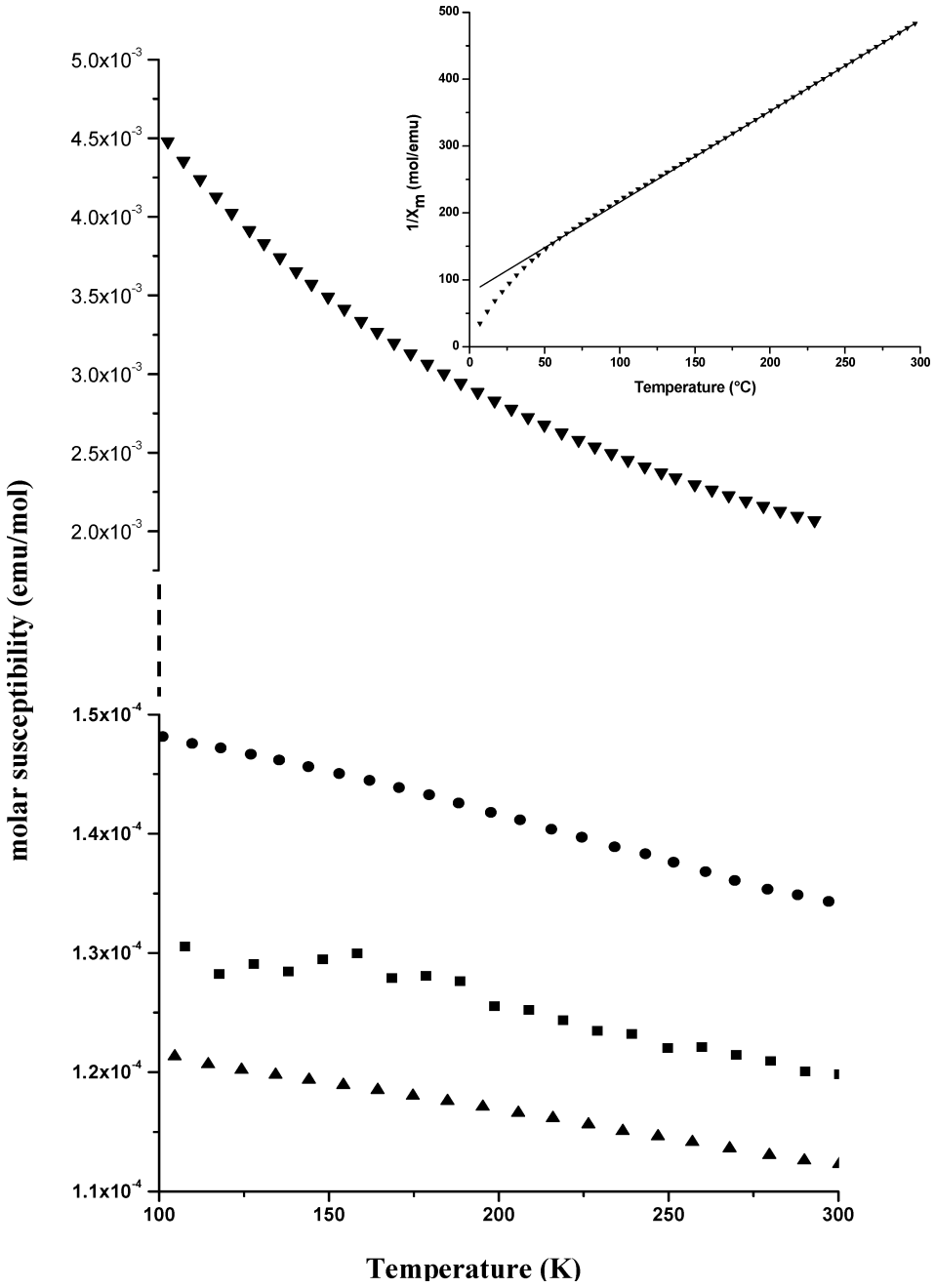

Figure 1. Variation of magnetic susceptibilities versus temperature of $Ce_{0.75}Ca_{0.25}O_{1.67}F_{0.17}$ (■), $Ce_{0.75}Ca_{0.25}O_{1.75}$ (●), $Ce_{0.91}Na_{0.09}O_{1.87}$ (▲), and CeF_3 (▼) (with thermal variation of the inverse susceptibility).

duration of the maturation of the oxyhydroxides: 3 h for F7 and 20 h for F6. In the former conditions, for high Ca content, the Ca^{2+} ions are probably not homogeneously distributed into the network. So, the introduction of fluorine ions in the mixture leads to the segregation of Ca atoms and finally to the formation of CaF_2. In the latter conditions, the duration of the oxide maturation induced indeed a better homogeneity of Ca^{2+} ions into the network of ceria. As F^- ions were introduced into the Ca−Ce matrix, the formation of CaF_2 was avoided, leading to Ca−Ce oxyfluorides with high Ca/Ce and F/Ce atomic ratios.

2. Ce Valence State in $Ce_{1-x}Ca_xO_{2-x}$ Oxides and in $Ce_{1-x}Ca_xO_{2-x-y/2}F_y$ Oxyfluorides Identified by Magnetic Measurements. To confirm the Ce valence state in Ce−Ca-based oxides and oxyfluorides after the coprecipitation and the thermal treatment at 600 °C under air, magnetic measurements were carried out on $Ce_{0.91}Na_{0.09}O_{1.87}$, $Ce_{0.75}Ca_{0.25}O_{1.75}$, and $Ce_{0.75}Ca_{0.25}O_{1.67}F_{0.17}$ compounds. The thermal dependence of the molar magnetic susceptibility of these compounds and that of CeF_3 are presented in Figure 1. In Table 3, molar susceptibilities at 300 K of these samples after diamagnetic corrections are listed as well as those of $Ce_2Sn_2O_7$,[24] CeF_3, commercial CeO_2 from Alfa Products, and CeO_2 data reported in the literature.[25] In CeF_3 and $Ce_2Sn_2O_7$ compounds, cerium ions are totally in trivalent state, whereas they are totally in tetravalent state in CeO_2. The magnetic susceptibility of cerium trifluoride follows a Curie−Weiss

(24) Tolla, B.; Demourgues, A.; Isnard, O.; Menetrier, M.; Pouchard, M.; Rabardel, L.; Seguelong, T. *J. Mater. Chem.* **1999**, *9*, 3131−3136.
(25) Ratnasamy, P.; Srinivas, D.; Satyanarayana, C. V. V.; Manikandan, P.; Kumaran, R. S. S.; Sachin, M.; Shetti, V. N. *J. Catal.* **2004**, *221*, 455−465.

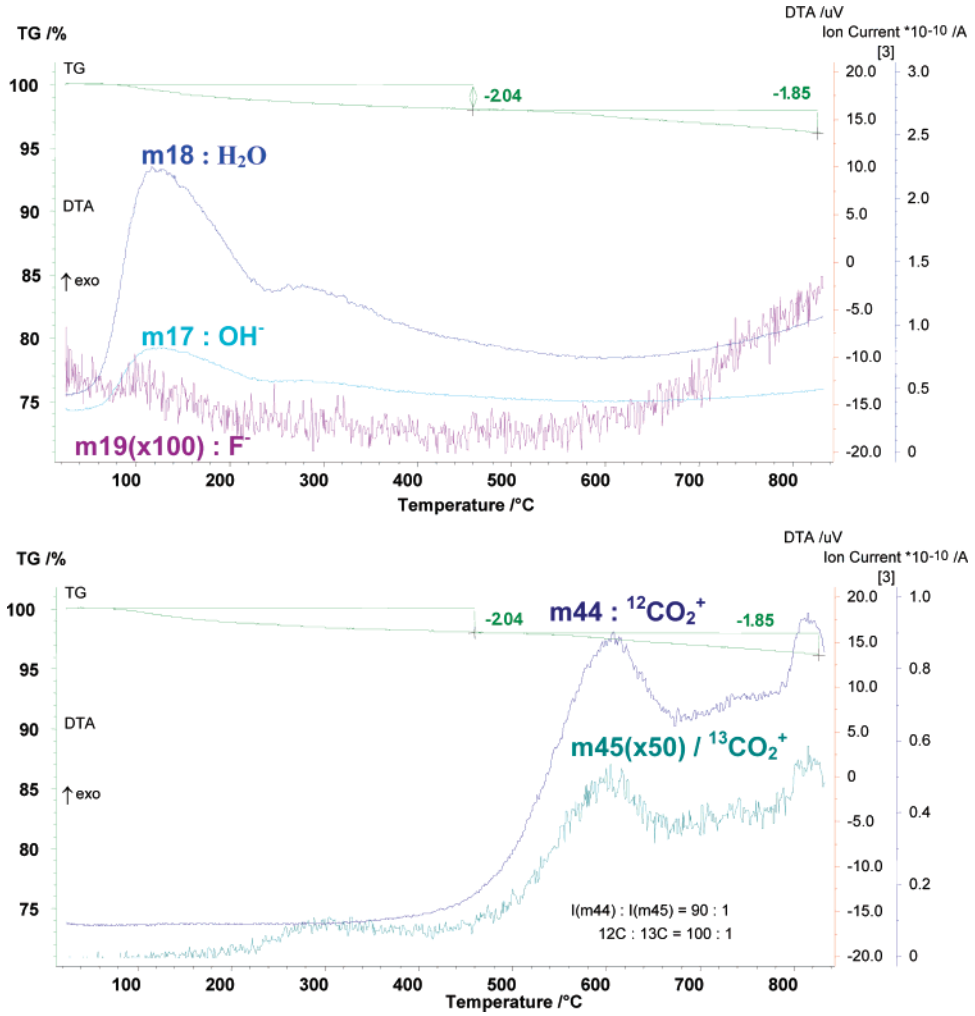

Figure 2. TGA-MS analysis of $Ce_{0.75}Ca_{0.25}O_{1.67}F_{0.17}$ composition (m = 44, 45: CO_2, m = 18, 17: H_2O, OH, and m = 19: F).

law versus the temperature (100 K ≤ T ≤ 300 K) with a theoretical effective magnetic moment equal to 2.54 μ_B/Ce atom (2.43 μ_B/Ce atom for the experimental value). CeO_2 is assumed to be diamagnetic; its magnetic susceptibility is equal to 0.6×10^{-4} emu/mol and is almost 50 times lower than those of CeF_3 and $Ce_2Sn_2O_7$ compounds. Figure 1 shows that the Ce−Ca-based oxides and oxyfluorides have approximately the same thermal dependence of the magnetic susceptibility with the same order of magnitude. The comparison of their magnetic susceptibilities with paramagnetic and diamagnetic references in Table 3 but also in Figure 1 reveals that the Ce^{3+} content is so low that it cannot be determined. Moreover, the ^{19}F MAS NMR study, mentioned in the solubility limit section, confirms also the absence of any dipolar broadening between fluorine ions and Ce^{3+} ions, leading one to consider that the majority of cerium ions are in the tetravalent state. Therefore, as the cerium are considered only in tetravalent state in Ce−Ca-based oxides and oxyfluorides, the following formula can be proposed for these systems: $Ce_{1-x}Ca_xO_{2-x}$ for the oxides and $Ce_{1-x}Ca_xO_{2-x-y/2}F_y$ for the oxyfluorides.

3. Thermal Behavior. Thermogravimetry analysis coupled with mass spectrometry TGA-MS was performed on $Ce_{0.75}Ca_{0.25}O_{1.67}F_{0.17}$ compound as shown in Figure 2. Two main regions were detected. The first weight loss attributed to H_2O departure occurs below T = 150 °C, and the second one is observed around 450 and 850 °C and is attributed to HF and CO_2 departures. HF loss starts from 600 °C and CO_2 starts from 450 °C. The departure of carbon dioxide suggests the presence of carbonate species into the sample associated with Ce^{4+} and Ca^{2+} ions as it has been already reported.[17,26] After gas chromatography analysis, the C content was estimated in this sample around 1.6 wt %.

Only TGA analyses were performed on $Ce_{0.87}Ca_{0.13}O_{1.86}F_{0.03}$, $Ce_{0.80}Ca_{0.20}O_{1.77}F_{0.07}$, and $Ce_{0.71}Ca_{0.29}O_{1.59}F_{0.24}$ compositions and are presented in Figure 3. The two regions mentioned just before were also observed for these three compounds, and it appears that the total weight loss observed at 800 °C increases with the Ca content: 3.9, 5.2, and 7.8 wt % for compounds with the molar ratio Ca/Ce = 0.15, 0.25, and 0.41, respectively. Whereas the water loss seems to be always between 2 and 3 wt %, the HF and CO_2 rates increase strongly with the Ca content. This feature is in good agreement with the increase of the Ca content into these compositions associated with the presence of carbonate and fluoride ions.

(26) Wolf, D.; Heber, M.; Grünert, W.; Muhler, M. *J. Catal.* **2001**, *199*, 92−106.

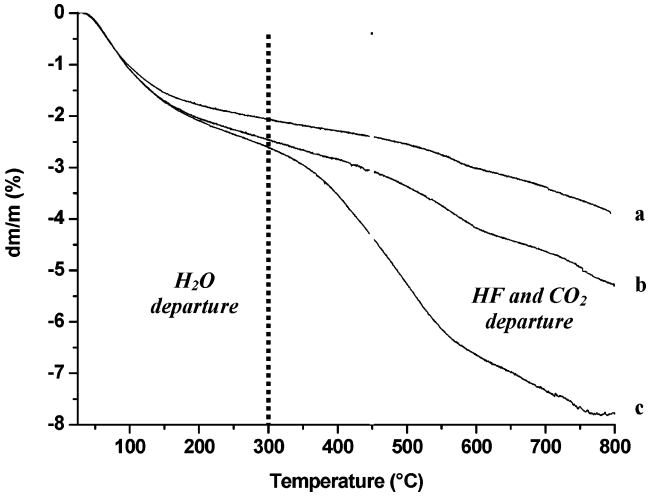

Figure 3. Thermogravimetry analysis of (a) $Ce_{0.87}Ca_{0.13}O_{1.86}F_{0.03}$, (b) $Ce_{0.80}Ca_{0.20}O_{1.77}F_{0.07}$, and (c) $Ce_{0.71}Ca_{0.29}O_{1.59}F_{0.24}$ compositions.

4. Structural Analysis of $Ce_{1-x}Ca_xO_{2-x}$ and $Ce_{1-x}Ca_xO_{2-x-y/2}F_y$ Compositions. For each sample, a powder X-ray diffraction analysis was carried out to determine the cell parameter evolution and to control the phase purity. Figure 4 shows the diffractograms of $Ce_{0.91}Na_{0.09}O_{1.87}$, $Ce_{0.87}Ca_{0.13}O_{1.86}F_{0.03}$, $Ce_{0.75}Ca_{0.25}O_{1.67}F_{0.17}$, and $Ce_{0.71}Ca_{0.29}O_{1.59}F_{0.24}$ compositions. The position and intensity of diffraction peaks are in good agreement with a cubic symmetry with the $Fm\bar{3}m$ space group related to fluorite-type structure. This structure can be described (Figure 5) as a fcc array of cerium ions in cubic symmetry with oxygens occupying all of the tetrahedral sites. Figure 4 reveals a shift to lower 2θ values of the diffraction lines for increasing Ca/Ce atomic ratios. This feature is due to the increase of the cell parameters resulting from the Ca^{2+} substitution for Ce^{4+} ions and as a consequence of the larger ionic radius for Ca^{2+} as compared to Ce^{4+}: 1.12 and 0.97 Å,[27] respectively, for 8-fold coordination number. The *a* lattice parameters are listed in Table 4 and range from 5.4077 (1) Å for Ca/Ce = 0 and F/Ce = 0 to 5.4217 (4) Å for Ca/Ce = 0.41 and F/Ce = 0.34. These values are approximately between the cell parameters of CeO_2 (5.41 Å)[18] and CaF_2 (5.46 Å).[19] The evolution of the lattice parameters with the Ca atomic content in oxides and oxyfluorides is illustrated in Figures 6 and 7, respectively. The lattice parameters and the error bars were determined from the refinement as explained further. Both for oxides and for oxyfluorides the curves follow Vegard's law, thus confirming that Ca^{2+} have been substituted for Ce^{4+} ions.

In addition, the higher is the Ca content, the broader are the diffraction lines of the XRD patterns as shown in Figure 4. Indeed, the peaks of the $Ce_{0.71}Ca_{0.29}O_{1.59}F_{0.24}$ compound are twice broader than those of the $Ce_{0.91}Na_{0.09}O_{1.87}$ compound. The broadness of diffraction peaks results from two contributions: crystallite size and microstrains. So the crystallite size is very small (<20 nm) and decreases as the Ca/Ce atomic ratio rises as reported in Table 4. The *a* lattice parameters and τ_c crystallite sizes were determined by a profile matching using the Thompson−Cox−Hastings function (function 7 in Fullprof package). The Thompson−Cox−

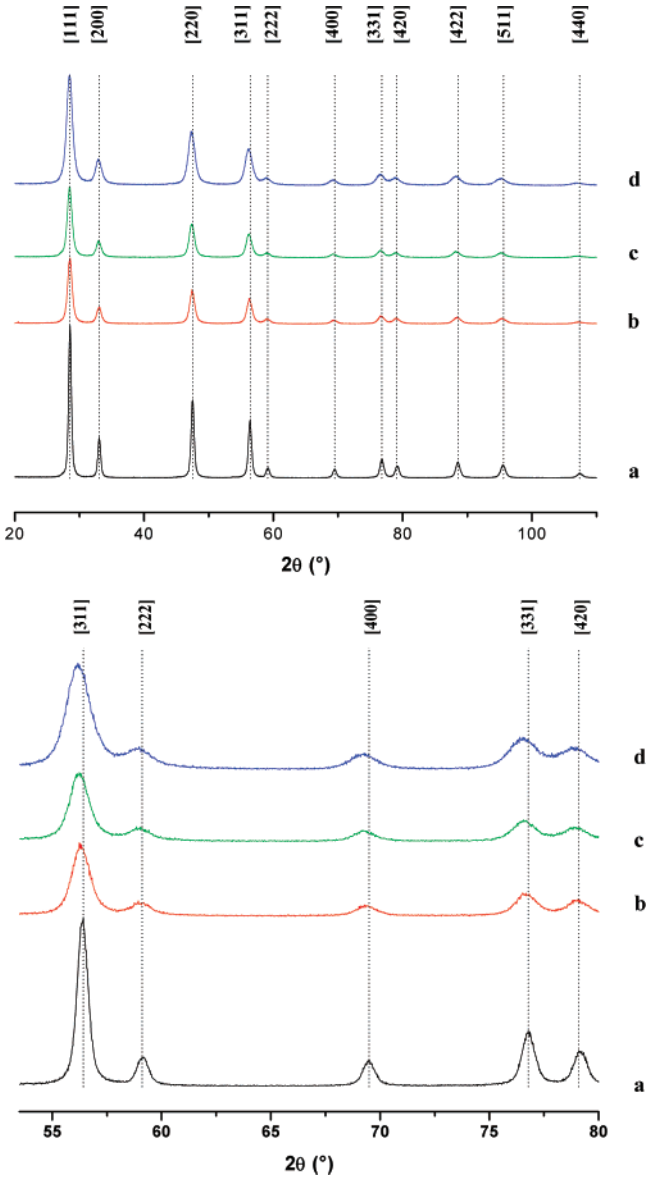

Figure 4. Powder X-ray diffraction patterns of (a) $Ce_{0.91}Na_{0.09}O_{1.87}$, (b) $Ce_{0.87}Ca_{0.13}O_{1.86}F_{0.03}$, (c) $Ce_{0.75}Ca_{0.25}O_{1.67}F_{0.17}$, and (d) $Ce_{0.71}Ca_{0.29}O_{1.59}F_{0.24}$ compositions.

Hastings function is often used to refine profiles with broad diffraction peaks because it is the more appropriate model for line broadening analysis where the Lorentzian and Gaussian contributions for crystallite size and for microstrains are weighted.[28] So, in this case, the peak shape is simulated by the pseudo-Voigt function, which is a linear combination of a Gaussian and a Lorentzian function (Table 5).

In the case of isotropic contributions, the line broadening is defined by two expressions:

$$H_G^2 = (U + DST^2)*\tan^2\theta + V*\tan\theta + W + IG/\cos^2\theta$$

$$H_L = X*\tan\theta + Y/\cos\theta$$

where H_G and H_L are the fwhm's of the Gaussian and Lorentzian profile components of the pseudo-Voigt function,

(27) Shannon, R. D. *Acta Crystallogr., Sect. A* **1976**, *32*, 751−767.

(28) Rodriguez-Carvajal, J.; Roisnel, T. Line broadening analysis using Fullprof. Materials Science Forum (European Powder Diffraction Conference; EPDIC8, Uppsala, 2002).

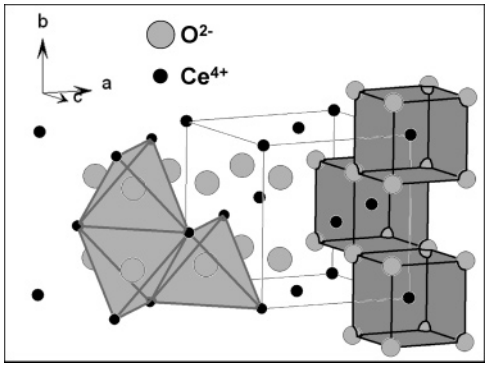

Figure 5. Fluorite-type structure of CeO_2 with cerium and oxygen environments.

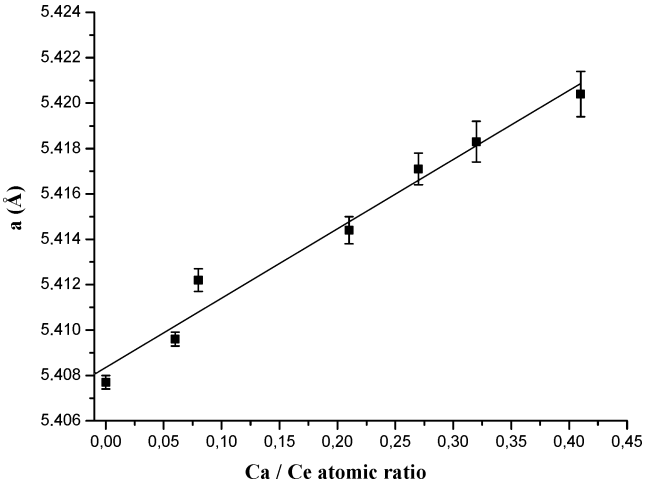

Figure 6. Dependence of the lattice parameter on the Ca atomic content in Ce−Ca-based oxides.

respectively. *U*, *V*, and *W* describe the instrumental profile. The Gaussian instrumental contribution follows Caglioti's law:[29]

$$H_{\mathrm{ins,G}}{}^2 = U^*\tan^2\theta + V^*\tan\theta + W$$

where *U*, *V*, and *W* are defined by refining in the same conditions a reference sample such as LaB_6 with large coherent diffraction domains. $IG/\cos^2\theta$ and $Y/\cos\theta$ represent the Gaussian and Lorentzian contributions, respectively, from isotropic crystallite size, and $DST^*\tan\theta$ and $X^*\tan\theta$ represent the Gaussian and Lorentzian contributions, respectively, from microstrain effects. The profile matching data and experimental conditions for data collection are summarized in Table 5.

The refinement of oxide as well as oxyfluoride diffractograms has shown that line broadening is not due to the Gaussian contribution of microstrains ($DST^*\tan\theta = 0$). The profile matching of diffractograms leads to the determination of lattice parameters *a* and crystallite sizes τ_c (see Table 4). The crystallite sizes vary from 16 to 7 nm and decrease when the Ca/Ce atomic ratio rises but are of the same order of magnitude for oxides and oxyfluorides for a same Ca/Ce atomic ratio. The estimated standard deviations corrected with the Berar's factor[30] are given in parentheses. The error

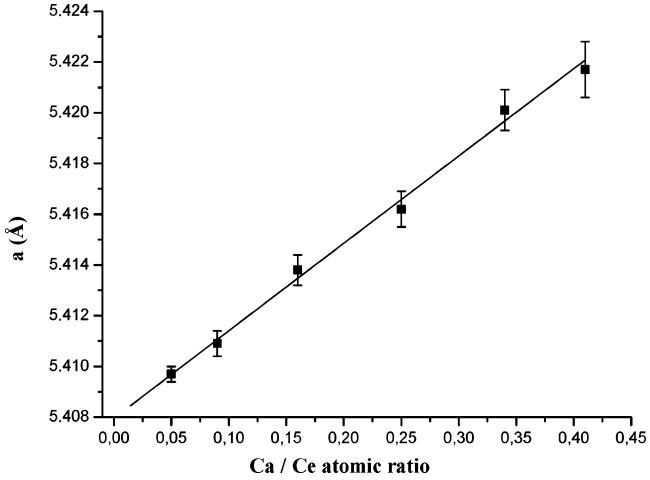

Figure 7. Dependence of the lattice parameter on the Ca atomic content in Ce−Ca-based oxyfluorides.

bars (see Figures 6 and 7) are deduced from the standard deviation.

The stabilization of Ca^{2+} and F^- ions into the Ce-based oxides adopting a fluorite-type structure with nanosized particles can then be explained. In many cases, alkaline or alkaline earth as well as fluorine are generally excellent sintering agents, which contribute to the particle growth. In the $Ce_{1-x}Ca_xO_{2-x}$ and $Ce_{1-x}Ca_xO_{2-x-y/2}F_y$ series, the particle size does not increase and remains around 10 nm. The electronegativity, formal charge, and ionic radius are indeed quite different for Ce^{4+} and Ca^{2+} ions from those of O^{2-} and F^- anions. Ca^{2+} cations are constrained to be 6-fold coordinated to oxygen as in CaO,[31] whereas Ce^{4+} ions prefer the cubic coordination as in CeO_2 leading to the stabilization of anionic vacancies and the formation of defects as well as dislocations. Moreover, the O coordination number varies from 6 in CaO to 4 in CeO_2, whereas the F coordination number changes from 4 in CaF_2 to 2 in CeF_4[32] and the cation−anion bond distances can vary on a large scale from 2.20 to 2.50 Å depending on the nature of ions. Such variations can explain the stabilization of such compositions and the occurrence of strong constrains in the network maintaining nanosized particles.

Figure 8 shows the evolution of strains with the atomic ratio Ca/Ce for the Ce−Ca-based oxides and oxyfluorides. The strain parameters were determined from the profile matching using the Thompson−Cox−Hastings function. For Ce−Ca-based oxides and oxyfluorides, the strains are given only by the Lorentzian contribution: $X^*\tan\theta$. A recent study by Rodriguez et al.[17] has shown that the Ca^{2+} substitution for Ce^{4+} ions in $Ce_{1-x}Ca_xO_{2-x}$ nanoparticles prepared by microemulsion method induced stress into the lattice due to the differences between Ce^{4+} and Ca^{2+} ion features like size, charge, and usual coordination number. Next, it has been demonstrated that the strains into the lattice increase with the Ca content and are consequently attributed to oxygen vacancies. This trend is also observed for $Ce_{1-x}Ca_xO_{2-x}$ and $Ce_{1-x}Ca_xO_{2-x-y/2}F_y$ compounds prepared by coprecipitation

(29) Caglioti, G.; Paoletti, A.; Ricci, F. P. *Nucl. Instrum. Methods* **1958**, *3*, 223−228.
(30) Bérar, J. L.; Lelann, H. *J. Appl. Crystallogr.* **1991**, *24*, 1−5.
(31) Ganguly, R.; Siruguri, V.; Gopalakrishnan, I. K.; Yakhmi, J. V. *J. Phys.: Condens. Matter* **2000**, *12*, 1683−1689.
(32) Schmidt, R.; Müller, B. G. *Z. Anorg. Allg. Chem.* **1999**, *625*, 605−608.

Table 4. Lattice Parameters *a* and Crystallite Size τ_c Determined from Powder XRD Diffractograms of Ce−Ca-Based Oxides and Oxyfluorides

i	sample O*i*	*a* (Å)	τ_c (nm)	sample F*i*	*a* (Å)	τ_c (nm)
1	$Ce_{0.91}Na_{0.09}O_{1.87}$	5.4077(1)	15	$Ce_{0.92}Ca_{0.05}Na_{0.03}O_{1.91}F_{0.00}$	5.4097(1)	15
2	$Ce_{0.92}Ca_{0.05}Na_{0.03}O_{1.91}$	5.4096(1)	16	$Ce_{0.91}Ca_{0.08}Na_{0.01}O_{1.90}F_{0.02}$	5.4109(2)	9
3	$Ce_{0.91}Ca_{0.07}Na_{0.02}O_{1.90}$	5.4122(2)	11	$Ce_{0.87}Ca_{0.13}O_{1.86}F_{0.03}$	5.4138(2)	10
4	$Ce_{0.83}Ca_{0.17}O_{1.83}$	5.4144(2)	10	$Ce_{0.80}Ca_{0.20}O_{1.77}F_{0.07}$	5.4162(2)	9
5	$Ce_{0.79}Ca_{0.21}O_{1.79}$	5.4171(2)	9	$Ce_{0.75}Ca_{0.25}O_{1.67}F_{0.17}$	5.4201(3)	9
6	$Ce_{0.75}Ca_{0.25}O_{1.75}$	5.4183(3)	7	$Ce_{0.71}Ca_{0.29}O_{1.59}F_{0.24}$	5.4217(4)	7
7	$Ce_{0.71}Ca_{0.29}O_{1.71}$	5.4204(3)	7	$Ce_{1-x}Ca_xO_{2-x-y/2}F_y + CaF_2$	5.4213(3)	9

Table 5. Profile Matching Data and Experimental Conditions for Data Collection

symmetry	cubic
space group	$Fm\bar{3}m$
radiation	Cu K_α ($\lambda = 1.5418$ Å) graphite monochromator
peak shape function	pseudo-Voigt function using the Thompson−Cox−Hastings formulas
fwhm function	$H_G^2 = (U + DST^2)\tan^2\theta + V\tan\theta + W + IG/\cos^2\theta$ $H_L = X\tan\theta + Y/\cos\theta$
reflections collected − 2θ range (deg)	11-5 < 2θ < 110
parameters used in refinement	13

in basic medium. Indeed, Figure 8 illustrates that the strains into the structure are more important for compounds with high Ca content. Moreover, the comparison between Ce−Ca-based oxides and oxyfluorides with the same Ca/Ce atomic ratio and almost the same crystallite size reveals that the fluorination of the oxides seems to reduce the strains into the network (comparison of samples $Ce_{0.75}Ca_{0.25}O_{1.75}$ and $Ce_{0.75}Ca_{0.25}O_{1.67}F_{0.17}$, as well as samples $Ce_{0.71}Ca_{0.29}O_{1.71}$ and $Ce_{0.71}Ca_{0.29}O_{1.59}F_{0.24}$). As it has been developed in the previous paragraph, the Ca^{2+} substitution for Ce^{4+} leads to the creation of oxygen vacancies into the lattice. These vacancies contribute to the strain formation. The number of vacancies and consequently the strains increase when the Ca/Ce atomic ratio rises and decrease when these anionic vacancies are partially filled with fluorine atoms.

5. CaF_2 Observation and Solubility Limit of Ca^{2+} and F^- Ions into Ceria. Because of the important width of diffraction peaks and the very close cell parameters of CeO_2 and CaF_2 (5.41 and 5.46 Å, respectively), an XRD analysis with monochromatic Cu K_{α_1} radiation is necessary to detect the presence of CaF_2 in the sample. An example is proposed for a sample whose elemental analysis has given 29 mol % Ca^{2+} and 36 mol % F^- (sample F7). It is interesting to notice that the CaF_2 phase cannot be identified when the XRD data are recorded using Cu K_{α_1} and Cu K_{α_2} radiations (Figure 9), whereas CaF_2 can be detected when the XRD data are obtained without Cu K_{α_2} radiation (Figure 10).

In the same manner, a diffractogram without the Cu K_{α_2} radiation was recorded for $Ce_{0.71}Ca_{0.29}O_{1.59}F_{0.24}$ composition, confirming the absence of calcium fluoride (Figure 10). This study reveals that the limit of solubility corresponds to a Ca/Ce atomic ratio around 0.40 for both oxyfluoride and oxide series.

As it has been previously mentioned for $Ce_{0.71}Ca_{0.29}O_{1.59}F_{0.24}$ composition (sample F6), a long maturation of particles of oxyhydroxides (20 h as compared to 3 h for the sample F7) prevents the formation of CaF_2. A simple ionic model without anionic vacancies shows that the ionic ratio

$$r_{\text{cations}}/r_{\text{anions}} = \sqrt{3} - 1 \qquad \text{(i)}$$

corresponds to the theoretical limit of a cubic close-packed of cations in which anions occupy tetrahedral holes. The cationic radii in oxygen environment, which are present in majority in a cubic coordination without anionic vacancies, are $r_{Ce^{4+}} = 0.97$ Å and $r_{Ca^{2+}} = 1.12$ Å (Shannon[27]), and the O^{2-} radius in 4-fold coordination in fluorite-type structure is $r_{O^{2-}} = 1.38$ Å. The (i) expression thus becomes

$$\frac{x\cdot r_{Ce^{4+}} + (1-x)\cdot r_{Ca^{2+}}}{r_{O^{2-}}} = \sqrt{3} - 1 \qquad \text{(ii)}$$

leading to $x = 0.73$ for the limit composition. In these conditions, the corresponding composition $Ce_{0.73}Ca_{0.27}O_{1.73}$ is very close to the as-prepared $Ce_{0.71}Ca_{0.29}O_{1.71}$ compound. Considering now a O^{2-} ionic radius of 1.40 Å, which is the common value used for such anions, an *x* limit value equal to 0.64 is obtained, corresponding to the following $Ce_{0.64}Ca_{0.36}O_{1.64}$ composition. It is then difficult to conclude about the Ca limit of solubility. Finally, one should have to point out when the Ca/Ce precursor content increases up to 1, a mixture of $Ce_{1-x}Ca_xO_{2-x}$ oxide and $CaCO_3$ is obtained. Moreover, in Ce−Ca-based oxides, the presence of Ca^{2+} ions leads to the creation of oxygen vacancies, and Ce^{4+} and Ca^{2+} cations can adopt various coordination numbers, probably between 6 and 8. On a steric point of view, the occurrence of oxygen vacancies contributes also to reduce the Ca limit of solubility.

In the case of fluorinated compounds, the F^- ionic radius in a tetrahedral coordination is always lower than one of O^{2-} ion: $r_{F^-} = 1.31$ Å.[27] In CaF_2, considering a cubic close-packed array with $r_{Ca^{2+}} = 1.12$ Å, a $r_{F^-} = 1.25$ Å is found, whereas in CeO_2 with $r_{Ce^{4+}} = 0.97$ Å, a $r_{O^{2-}} = 1.38$ Å is deduced. Next, the F^- substitution for O^{2-} should increase the Ca solubility limit, thanks on one hand to the theoretical reduction of global anionic radius but also because of the decrease of the number of anionic vacancies. It is then reasonable to consider that the Ca solubility limit is close to 0.3 corresponding both to $Ce_{0.7}Ca_{0.3}O_{1.7}$ and to $Ce_{0.7}Ca_{0.3}O_{1.58}F_{0.25}$ limit compositions.

Furthermore, to conclude definitively about the presence of CaF_2 as mentioned by powder XRD analysis as well as the large content of fluorine ions and their introduction into the vicinity of calcium and cerium IV ions, ^{19}F NMR study has been undertaken on two samples, F6 ($Ce_{0.71}Ca_{0.29}O_{1.59}F_{0.24}$) and F7 ($Ce_{1-x}Ca_xO_{2-x-y/2}F_y + CaF_2$). Figure 11 shows the ^{19}F MAS NMR spectra of these two samples. Four broad

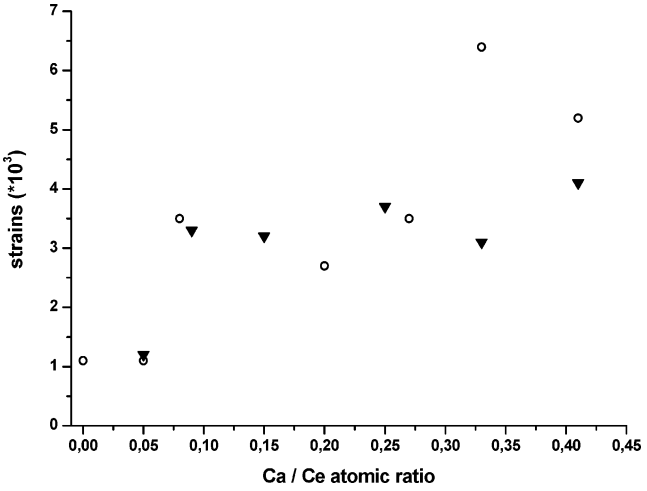

Figure 8. Evolution of microstrains with Ca/Ce atomic ratio for Ce−Ca-based oxides (○) and oxyfluorides (▼).

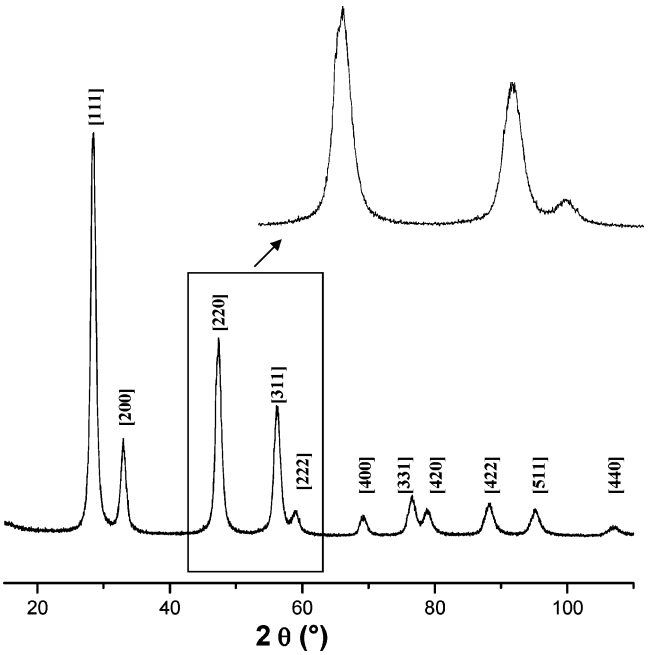

Figure 9. Powder X-ray diffraction pattern of $Ce_{1-x}Ca_xO_{2-x-y/2}F_y + CaF_2$ sample obtained with Cu K_α radiations (K_{α_1} and K_{α_2}).

peaks are observed, for F6 and F7. The δ_{iso} values and the relative intensities are gathered in Table 6. These δ_{iso} values are nearer to the ^{19}F δ_{iso} value in CaF_2 (58 ppm[33]) than those in CeF_4 (360−400 ppm[34]). They may be related to $Ca_{4-x}Ce_x$ tetrahedron fluorine environments with x increasing from 0 to 3 with ^{19}F δ_{iso} (Table 6). From these results, it appears that the main fluorine environment, in these two samples, is FCa_2Ce_2 tetrahedron, and those of FCe_4 do not exist around fluorine ions. Moreover, for F7, there is a weak additional peak at 59 ppm in good agreement with the presence of a small quantity of CaF_2 impurity identified also by XRD. The dependence of the ^{19}F NMR data on the compositions will be discussed in detail in a forthcoming paper. Moreover, the ^{19}F MAS NMR spectra do not exhibit any dipolar broadening

(33) Bureau, B.; Silly, G.; Buzaré, J.-Y.; Emery, J. *Chem. Phys.* **1999**, *249*, 89−104.

(34) Legein, C.; Fayon, F.; Martineau, C.; Body, M.; Buzaré, J.-Y.; Massiot, D.; Durand, E.; Tressaud, A.; Demourgues, A.; Péron, O.; Boulard, B. *Inorg. Chem.* **2006**, *45*, 10636−10641.

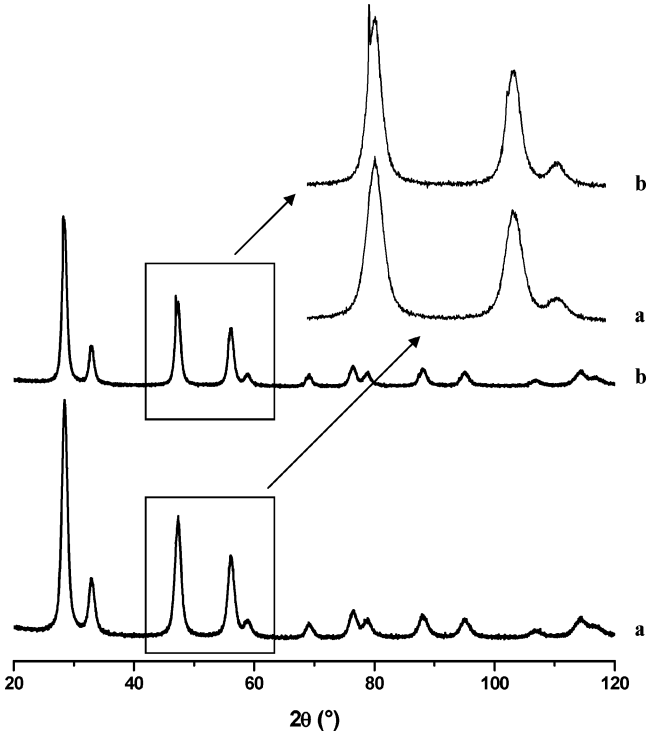

Figure 10. Powder X-ray diffraction pattern of (a) $Ce_{0.71}Ca_{0.29}O_{1.59}F_{0.24}$ and (b) $Ce_{1-x}Ca_xO_{2-x-y/2}F_y + CaF_2$ samples obtained with monochromated Cu K_α radiation (K_{α_1}).

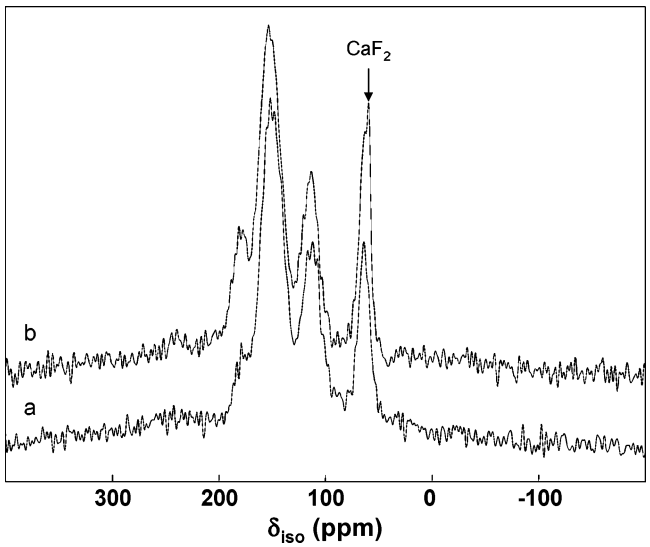

Figure 11. ^{19}F MAS NMR spectra of (a) F6: $Ce_{0.71}Ca_{0.29}O_{1.59}F_{0.24}$ and (b) F7: $Ce_{1-x}Ca_xO_{2-x-y/2}F_y + CaF_2$ samples at 25 kHz. The arrow points out the resonance attributed to CaF_2.

between fluorine ions and Ce^{3+} ions, confirming that the cerium is only in tetravalent state in the Ce−Ca-based oxyfluorides.

6. TEM and EELS Analysis: Particle Size and Composition of Nanoparticles. The particle size and the morphology were studied by transmission electron microscopy (TEM) on $Ce_{0.75}Ca_{0.25}O_{1.67}F_{0.17}$ (sample F5). The morphology is not homogeneous, whereas the particle sizes are quite identical. Figure 12 shows particles of about 10 nm, which is similar to the crystallite size determined by XRD analysis. The images lead one to conclude that the particles are monocrystalline.

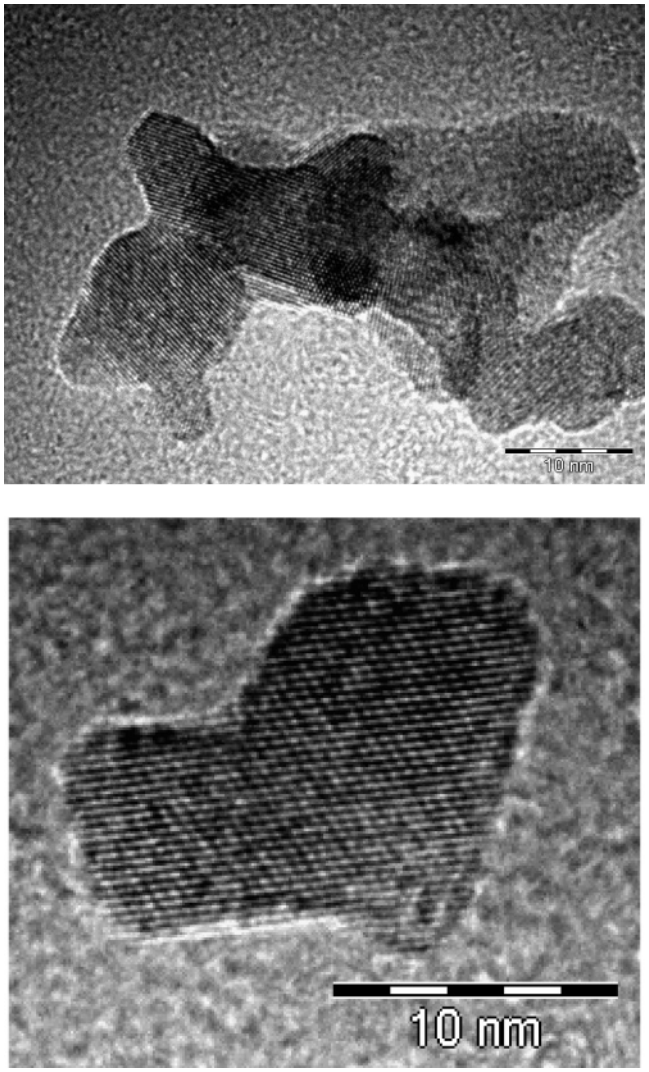

Figure 12. High-resolution TEM images (200 kV) of $Ce_{0.75}Ca_{0.25}O_{1.67}F_{0.17}$ composition, agglomerated particles (top), and single particle (bottom).

Table 6. δ_{iso} (ppm) and Relative Intensities (%) As Deduced from NMR Spectrum Simulations and Fluorine Environments for Samples F6 and F7

F6 ($Ce_{0.71}Ca_{0.29}O_{1.59}F_{0.24}$)		F7 ($Ce_{1-x}Ca_xO_{2-x-y/2}F_y + CaF_2$)		
δ_{iso} (±1)	intensity (±0.5)	δ_{iso} (±1)	intensity (±0.5)	environment
63.5	12.9	63	15.3	Ca_4
113.5	28.3	114	23.3	Ca_3Ce
150.5	47.8	152	44.1	Ca_2Ce_2
179	11.0	180	15.0	$CaCe_3$
		59	1.3	CaF_2

Energy electron-loss spectroscopy (EELS) experiments were performed on isolated particles of $Ce_{0.75}Ca_{0.25}O_{1.67}F_{0.17}$. Figure 13 illustrates EELS spectra realized on two isolated particles showing that the four elements have been detected even if the F−K edge is very low because the F/O atomic ratio is close to 0.1. The Ca/Ce average atomic ratio was evaluated on isolated nanoparticles to 0.30 with a standard deviation of 0.04. This value corresponds to the ratio deduced from microprobe analysis: Ca/Ce = 0.342(8). Furthermore, EELS analysis on isolated nanoparticles of $Ce_{0.75}Ca_{0.25}O_{1.75}$ oxide reveals also the quite good homogeneity of the oxide with a molar ratio Ca/Ce = 0.29 and a standard deviation of 0.04. EELS experiments have confirmed the good Ca/Ce homogeneity at the nanoparticle level in both oxide and oxyfluoride systems.

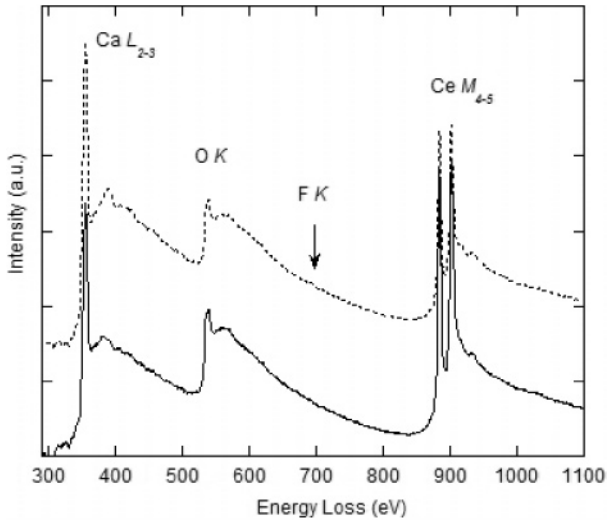

Figure 13. EELS spectra showing the Ce $M_{4,5}$-, Ca $L_{2,3}$-, O, and F K-edges of $Ce_{0.75}Ca_{0.25}O_{1.67}F_{0.17}$ composition recorded on two single grains.

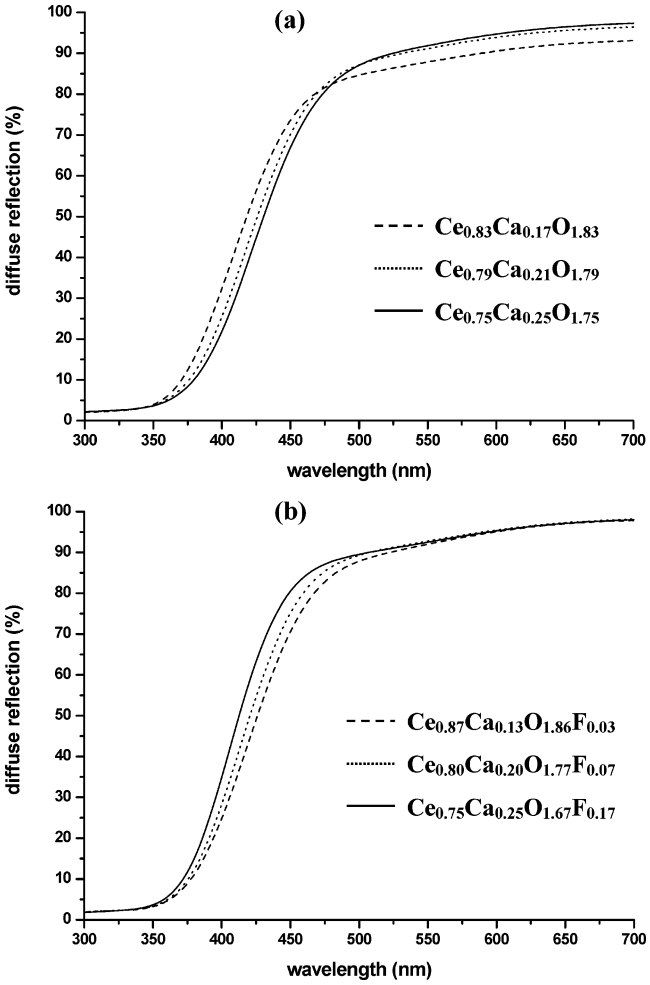

Figure 14. UV−visible diffuse reflectance spectra of Ce−Ca-based (a) oxides and (b) oxyfluorides.

In the $Ce_{1-x}Ca_xO_{2-x-y/2}F_y$ series, the F content varies but the F/Ca atomic ratio is always lower than 1. On the basis of a random distribution of cations and anions in cubic close-packed array and considering that F^- is 2-fold coordinated to Ce^{4+} in CeF_4 and 4-fold coordinated to Ca^{2+} in CaF_2, it

is clear that F^- ions have probably a strong preference for Ca^{2+} ions in tetrahedral coordination. As the F^- ions are 4-fold coordinated to Ca^{2+}/Ce^{4+} cations in $Ce_{1-x}Ca_xO_{2-x-y/2}F_y$ compounds with a F/Ca atomic ratio always lower than 1, the F^- ions will be predominantly surrounded by two Ca^{2+} and two Ce^{4+} cations. This point will be discussed in a forthcoming paper.

7. UV-Shielding Properties. The diffuse reflectance spectra of various oxides, $Ce_{0.83}Ca_{0.17}O_{1.83}$, $Ce_{0.79}Ca_{0.21}O_{1.79}$, and $Ce_{0.75}Ca_{0.25}O_{1.75}$, and oxyfluorides, $Ce_{0.87}Ca_{0.13}O_{1.86}F_{0.03}$, $Ce_{0.80}Ca_{0.20}O_{1.77}F_{0.07}$, and $Ce_{0.75}Ca_{0.25}O_{1.67}F_{0.17}$, are given in Figure 14a,b. One has to point out the interesting UV-shielding properties of these compounds with absorption edge around 400 nm and lower refractive index and high transparency in visible range in the case of $Ce_{1-x}Ca_xO_{2-x-y/2}F_y$ compositions taking into account the Gladstone−Dale relationship with $n(CeO_2) = 2.50$, $n(CaO) = 1.80$, and $n(CaF_2) = 1.50$ at $\lambda = 550$ nm.

In the oxide series, the absorption edge relative to the charge-transfer band (CTB, 2p (O) → 4f (Ce)) shifts to the lowest energies as the Ca content increases. On the contrary, in the oxyfluoride series, the absorption edge moves to the highest energies as the Ca content raises. However, in a previous paragraph, it has been demonstrated that the fluorine content in the oxyfluoride series follows the Ca amount and the higher is the fluorine content, the higher is the optical band gap associated with the 2p (O) → 4f (Ce) CTB. The comparison of the optical band gap in CeO_2-fluorite and in $SrCeO_3$-perovskite equal to 3.1 (400 nm) and 3.5 eV (360 nm), respectively,[8] clearly shows that this evolution is governed by the Ce−O chemical bonding, that is, the coordination number and the Ce−O bond distances. In CeO_2-fluorite, the Ce^{4+} ions are 8-fold coordinated to oxygen atoms and Ce−O = 2.34 Å, whereas in perovskite $SrCeO_3$, Ce^{4+} ions are 6-fold coordinated to oxygen atoms and Ce−O = 2.25 Å, with an increase of the CTB energy. Such a trend is associated with the destabilization of 4f (Ce) band and to the strong stabilization of 2p (O) band as both coordination number and Ce−O bond distances decrease.

In the oxide series, the progressive introduction of Ca^{2+} cations into the network contributes to increase the oxygen vacancy rate, and thus reduces the average cationic coordination number. On the other hand, the higher is the Ca content, the higher is the *a*-cell parameter relating to the expansion of the framework and the average bond distances. Next, it is reasonable to consider that in the oxide series, Ca^{2+} cations tend to occupy 6-fold coordinated sites as in CaO where Ca−O bond distances lie around 2.40 Å, leaving Ce^{4+} cations with higher coordination number than Ca^{2+} cations and large Ce−O bond distances. In other terms, in $Ce_{1-x}Ca_xO_{2-x}$ oxides, Ca^{2+} cations force Ce^{4+} cations to become less electropositive than in CeO_2 by adopting a coordination number smaller than 8 and larger bond distances. Thus, in the oxide series, the higher is the Ca content, the less electropositive are the Ce^{4+} cations, leading to the reduction of the energy of 2p (O) → 4f (Ce) CTB.

In the oxyfluoride series, considering the same amount of Ca^{2+} ions, the number of anionic vacancies is smaller because of the presence of fluorine ions substituting for O^{2-} ions, and the band gap energy varies conversely to the trend observed in the oxide series. For $Ce_{1-x}Ca_xO_{2-x-y/2}F_y$ compositions, Ca^{2+} ions because of their strong preference for F^- ions occupy probably 8-fold coordinated sites with a large amount of fluorine surrounding Ca^{2+} cations, leaving Ce^{4+} ions with a lower coordination number and fluorine in its vicinity. Next, Ca^{2+} and F^- ions constrain Ce^{4+} cations to be more electropositive than in CeO_2, leading to stabilize more the 2p(O) valence band with regard to the 4f(Ce) level. The higher are the Ca and F contents in this series, the more pronounced is the ionic character of Ce−O chemical bonding, leading to an increasing of the optical band gap. It has been thus demonstrated how a high electropositive cation such as Ca^{2+} and a high electronegative anion such as F^- are able to tune the 2p(O) → 4f(Ce) CTB energy or the band gap energy in Ce−Ca-based oxides.

Finally, one should have to point out that the optical absorption properties of the system containing both CaF_2 and $Ce_{1-x}Ca_xO_{2-x-y/2}F_y$ compounds have not been investigated. Only pure phases corresponding to specific compositions have been studied.

Conclusion

New $Ce_{1-x}Ca_xO_{2-x-y/2}F_y$ compositions have been prepared from coprecipitation of Ce−Ca salts in basic fluorinated medium (pH > 12). Magnetic measurements lead one to conclude about the absence of Ce^{3+} paramagnetic species, whereas TGA measurements allow one to show the affinity of these compounds with water and carbonates, which increases together with Ca content. The occurrence of Vegard's law for $Ce_{1-x}Ca_xO_{2-x}$ and $Ce_{1-x}Ca_xO_{2-x-y/2}F_y$ series and the appearance of CaF_2 lead one to conclude about the solubility limit corresponding to 30% of Ca^{2+} ions both for oxides and for oxyfluorides. Size particles are around 10 nm, and accurate EELS measurements demonstrate the rather good homogeneity in chemical composition of nanosized particles. ^{19}F NMR investigations show the occurrence of various fluorine environments depending on the nature of cations (Ce^{4+}/Ca^{2+}) and will be discussed in a forthcoming paper.

The presence of Ca^{2+} ions in CeO_2 fluorite network allows the creation of oxygen vacancies whose rate can be reduced by the presence of F^- ions substituting O^{2-} ions with a lower charge and a higher electronegativity. Moreover, the Ca^{2+} substitution in both these oxide and oxyfluoride series leads to an expansion of the unit cell and of the average Ce(Ca)−O(F) bond distances, despite the formation of oxygen vacancies, with respect to the larger ionic size of Ca^{2+} ions in 8-fold coordination. Furthermore, the preference of Ca^{2+} ions for F^- anions seems to be clear because of the high electronegativity and the tetrahedral coordination of F^- in CaF_2. Next, considering that F/Ca atomic ratio is always inferior to 1 for high Ca contents, the FCa_2Ce_2 sites have to be considered as the main environment for F^- anions as shown by preliminary ^{19}F NMR results. Moreover, the F amount increases with increasing Ca content, illustrating the strong affinity of fluorine for Ca atoms.

On the basis of an ionic model with a cubic close-packed array of cations with anions in tetrahedral holes and taking

into account the respective ionic radii, the theoretical solubility limit has been evaluated around 30% mol Ca. In the case of oxyfluoride series, the high stability of CaF_2 is the limiting factor for the incorporation of Ca^{2+} and F^- ions into the matrix.

Finally, the UV absorption properties show a reduction of the optical band gap as Ca content increases in the $Ce_{1-x}Ca_xO_{2-x}$ series, confirming results previously found.[16] The optical band gap increases with increasing Ca and F contents in the $Ce_{1-x}Ca_xO_{2-x-y/2}F_y$ series. The noteworthy evolution of the O (2p) → Ce (4f) charge-transfer band illustrates the versatility of Ce^{4+} ions to form various chemical bonding. In the case of oxides, the presence of Ca^{2+} ions forces Ce^{4+} ions to become less electropositive than in CeO_2 with an increase of the Ce−O bond lengths and a reduction of the band gap. In the case of oxyfluorides, the presence of both Ca^{2+} and F^- ions constrains Ce^{4+} ions to become more electropositive than in CeO_2 with an increasing of the optical band gap.

Acknowledgment. This paper is dedicated to Professor N. Bartlett on the occasion of his 75th birthday. This work has been supported by the Rhodia Co. We are particularly indebted to P. Dagault and L. Raison for their valuable assistance. We want to thank the CECM/CNRS laboratory (Vitry-sur-Seine, France) for their help on TEM images.

CM071482H